Frustration-induced diffusive scattering anomaly and unexpected dimension change in FeGe₂

- Yaokun Su¹, Hillary L. Smith², Matthew B. Stone³, Douglas L. Abernathy³, Mark D. Lumsden³, Carl P.
 Adams⁴, and Chen Li^{1,5*}
 - 1. Materials Science and Engineering, University of California, Riverside, Riverside, CA 92521, USA
 2. Physics and Astronomy, Swarthmore College, Swarthmore, PA 19081, USA
 - 3. Neutron Scattering Division, Oak Ridge National Laboratory, Oak Ridge, TN 37831, USA
 - 4. Department of Physics, St. Francis Xavier University, Antigonish, Nova Scotia B2G 2W5, Canada
 - 5. Mechanical Engineering, University of California, Riverside, Riverside, CA 92521, USA *chenli@ucr.edu

Abstract

- 12 Magnetic frustration, arising from the competition of exchange interactions, has received great attention
- because of its relevance to exotic quantum phenomena in materials. In the current work, we report an
- 14 unusual checkerboard-shaped scattering anomaly in FeGe₂, far from the known incommensurate magnetic
- satellite peaks, for the first time by inelastic neutron scattering. More surprisingly, such phenomenon
- appears as spin dynamics at low temperature, but it becomes prominent above Néel transition as elastic
- scattering. A new model Hamiltonian that includes an intraplane next-nearest neighbor was proposed and
- 18 attributes such anomaly to the near-perfect magnetic frustration and the emergence of unexpected two-
- dimensional magnetic order in the quasi-one-dimensional FeGe₂.

20

1 2

5

6

7

8

9

10

11

- 21 Magnetic frustration has attracted interest due to its relation to novel phases including quantum spin liquids,
- spin and electronic nematic phases and unconventional superconductivity [1–5]. Generally, the magnetic
- 23 frustration arises with special geometry of lattice, but it can also be achieved as a consequence of the
- competition between different pair antiferromagnetic (AFM) interactions.
- 25 In recent years, AFM materials have been widely studied due to their robustness again disturbance and
- potential applications in high density data storage [6], resistive switching [7,8] and spintronics [9,10]. As a
- 27 germanium-based AFM intermetallic, FeGe₂ has been explored by numerous experimental and theoretical
- studies for its complex magnetism [11–17]. Magnetic excitations have been measured in FeGe₂ [18,19],
- 29 revealing a large anisotropy and an overdamped feature of the spin wave. A NN Heisenberg model was
- 30 proposed with $SJ_c = 136$ meV and $SJ_1 = -8.8$ meV, where S is the on-site spin magnitude and Js are the
- 31 exchange constants. However, the measurements were highly restricted by the instruments used, and a
- 32 detailed examination of its magnetic excitations throughout the full Brillouin zone is still missing.
- 33 FeGe₂ has the same body-centered tetragonal crystal structure [20] (Fig. S1) as θ -phase Al₂Cu (space group
- 34 *I4/mcm*). It exhibits two zero-field magnetic phase transitions on heating [17,21]: one first-order transition
- 35 from a commensurate AFM state to an incommensurate spin-density-wave state at 263 K, and another
- second-order Néel transition from the incommensurate state to paramagnetic phase at 289 K. The ordering
- 37 wavevector changes from $(2\pi/a)[1, 0, 0]$ for the commensurate state to $(2\pi/a)[1+\delta, 0, 0]$ for the
- incommensurate state, where δ varies from 0 to 0.05. Along the c axis, the nearest neighbor (NN) distance
- between Fe atoms is 2.478 Å, which is close to that of elemental Fe (2.482 Å), such that ferromagnetic (FM)
- 40 exchange interaction J_c is expected to be strong. In the a-b plane, only a weak NN AFM exchange
- 41 interaction J₁ has been considered previously [18,19]. While the magnetic moments were known to lay in
- 42 the basal plane with a value of 1.2 μ_B per Fe atom, their exact orientation is still unclear [21].

43 Here we provide a combined scattering and computational study of FeGe₂ in examination of a portion of 44 the magnetic spectrum that was not previously identified. We use inelastic neutron scattering (INS) to 45 examine the lattice and magnetic dynamics of FeGe₂, revealing an unusual checkerboard-shaped scattering 46 anomaly. Such anomaly appears in dynamic part at low temperature and turns into diffusive intensity above Néel transition. An additional intraplane next-nearest neighbor (NNN) interaction J₂ is found to be 47 necessary to fully describe the spin wave spectrum. Exchange parameters calculated from atomistic 48 49 simulations and the new model including J₂ suggest the near-perfect magnetic frustration in FeGe₂, enabling 50 us to reproduce the anomalous excitation in the low temperature AFM state. Instead of the one-dimensional 51 (1D) correlation, unexpected two-dimensional (2D) correlations emerge as temperature increase, attributed 52 to the appearance of stripe-type domains and the magnetic frustration. Such 2D correlations are believed to 53 rationalize the anomalous checkerboard-shaped diffusive scattering.

A semi-cylindrical single crystal FeGe₂ with an approximate 15 mm radius and 40 mm length with a mass of 110 g was used for the INS measurements. This crystal, used in previous studies of FeGe₂ [19,22], was measured using ARCS and HB-3 at Oak Ridge National Laboratory (details in Supplemental Material).

57 Figure. 1 shows a sample of the INS data acquired as a function of both temperature and energy transfer. 58 Figs. 1(a)-1(b) shows the elastic scattering in the (HK0) planes. At 20 K, one sees the diffraction pattern 59 with several aluminum powder line rings visible (from sample environment background). As the 60 temperature increases, an anomalous feature can be observed clearly in the (HK0) slices of dynamical 61 structure factor S(Q, E) (Fig. 1 and Fig. S2). Besides the expected nuclear and magnetic Bragg peaks, there is extra intensity connecting NN magnetic Bragg peaks. This intensity forms a checkerboard arrangement 62 63 with rods along the X-M directions, as depicted in the 3D rendering at L = 0 (Fig. 1(1)). This checkerboard-64 shaped anomaly is found in both elastic and inelastic scattering slices and does not strongly depend on 65 energy transfer. At 20 K, such intensity can only be observed at finite energy transfers and appears to be 66 detached from M points, forming a dot-dash-dot pattern (Fig. 1(c)). TAX data at 8 meV shows that each 67 dash consists of two sections, which merge with the magnetic peaks at M points as the temperature increases 68 (Figs. 1(e)-(i)).

The extent of the phonon and magnetic excitation spectra can be assessed by examining the scattering intensity as a function of energy and momentum transfer along the X-M direction for 20 and 300 K as shown in Figs. 2 (a), 2(d) respectively. Magnetic excitations emerge from the M points and disperse up to approximately 30 meV. As momentum transfer increases, the magnetic form factor causes the spin wave scattering intensity to decrease. At larger momentum transfers, one can see the optical phonon excitations between approximately 15 and 35 meV.

Phonon simulations were performed using finite temperature effective force constants (details in Supplemental Material). The simulated phonons match well with experimental data, as shown in Figs. 2(b), 2(e) for X-M direction. The magnetic excitations dispersing out of M points were reproduced as described in Supplemental Material using the NN model, with SJ values from literature [19]. The NN model reproduce some other features of the magnetic spectrum. Along Γ-M direction, the simulated spin wave agrees perfectly with experimental data. Along X-M direction, the agreement is still good in the vicinity of the magnetic zone center, although the measured spin wave appears steeper (Fig. 2(c)).

There are important differences between the measurement and simulation. The main difference is that the continua-like intensity between neighboring M points is not reproduced in either phonon or spin wave simulation. This intensity is associated with the anomalous checkerboard intensity observed in the (HK0) planes. Although over-damped, this intensity can be resolved at 20 K as collective dispersive excitations, which reach the minimums at X points. At 300 K, this dispersive excitation is further damped and merges

87 to a broad response across a wide energy range along rod directions in the Brillouin zone. Spectral weight 88 perpendicular to this direction $(\Gamma - X)$ is weak and the dispersion is very steep around X points (Fig. S3).

89 To reveal the origin of the checkerboard anomaly, a Q-dependence analysis was performed. It is found this 90 anomalous intensity only appear where L is even (Fig. 1(k)), following the same behavior of magnetic 91 Bragg peaks. This observation indicates that the order behind the anomaly has the same periodicity along 92 the c axis as the magnetic structure of FeGe₂. To quantify the structural factor of the anomalous INS 93 intensity, equivalent points of [1.3, 0.3, 0] in momentum space were selected on each rod at 0 meV and 8 94 meV (HK0) slices and their intensity was compared to $AF^2(\mathbf{Q})+B$, where $F(\mathbf{Q})$ is the magnetic form factor 95 of charge-neutral Fe atom, A and B are constants to be fit. Fe atom was used here instead of ions since no 96 charge transfer was found in our charge distribution calculation [23]. Fig. 3 shows the excellent agreement 97 between the fitted curves and the experimental data, further confirming that the anomalous intensity, in 98 both the elastic and inelastic scattering, is indeed from the magnetic origin. At 20 K and 0 meV, as shown 99 in Fig. 3(a), the intensity is dominated by the background, consistent with the fact that no rod intensity was observed in the low temperature elastic scattering. Contributions to the checkerboard anomaly from other 100 sources including electronic scattering or leftover incommensurate order were considered but excluded, as 101 102 described in Supplemental Material.

To describe our observation, a new model is needed. A Checkerboard-shaped anomalous excitation without periodicity along [0, 0, L] has previously been observed in quasi-2D square lattice systems with magnetic frustration, and is described by the J₁-J₂ Heisenberg model [24,25]. Different from FeGe₂, the interlayer interaction J_c is ignored in these systems since it is generally much weaker. Besides the NN interaction J₁, the intraplane NNN interaction J₂ is also important in describing the excitations in these systems. The ground state of these systems could be determined by the frustration parameter $\eta = J_1/2J_2$, where J_1 could be either FM or AFM but J_2 is always AFM. Néel-type, stripe-type and FM ordering occurs for $\eta > 1$, $|\eta| <$ 110 1 and $\eta < -1$, respectively. Perfect frustration happens when $|\eta| = 1$. Extreme spatial anisotropy due to the perfect frustration leads to effectively 1D behavior and corresponding plane-like features in INS [26].

103

104

105

106

107

108 109

111

112 Identical to the magnetic atom in these systems, each Fe in FeGe2 has 4 intraplane NN atoms and 4 113 intraplane NNN atoms. However, FeGe₂ has an additional strong interplane interaction J_c. To determine the 114 extent of the role of J₂ interaction in FeGe₂, total energy calculations were made on five collinear magnetic 115 configurations and the exchange parameters were fit to these energies under the assumption that the change of energy is only dependent on the selected exchange interactions (Fig. S5 and Table SI). Two models were 116 used in the least-square fitting: the NN model containing only J₁ and J_c, and the NNN model that also 117 118 includes J₂. The results are shown in Error! Reference source not found..

119 For the NN model, the calculations yield $|J_0/J_1| \sim 11.6$, this large ratio represents the anisotropic nature of in-plane and Γ -Z spin waves in FeGe₂, consistent with previous report [18]. For the NNN model, J_1S^2 and 120 J_cS² remain almost unchanged from those values determined for the NN model and J₂S² has a value of -2.6 121 meV. J₁ and J₂ are of the same order of magnitude, indicating that both interactions play important roles in 122 123 describing the spin dynamics and should not be neglected.

Exchange parameters calculated for the NNN model were then used to perform spin wave simulations. 124 125 Assuming no charge transfer between Fe and Ge atoms and a low-spin configuration in a tetrahedral environment with spin S = 1 and g-factor of 2, the magnetic moment is expected to be $\mu =$ 126 $g\sqrt{S(S+1)}\mu_B = 2.8 \,\mu_B$ per Fe atom. However, this is about twice the experimental value, explained as 127 arising from hybridization of the 3d and 4s orbitals of the Fe atoms [14]. As a result, a smaller effective 128 129 value of S is needed to account for the itinerant nature of FeGe₂. A value of 0.5 was chose here so that spin 130 wave along Γ -M matches with result from literature [18]. The simulation in Fig. 2(f) shows the importance

- of J_2 in reducing the spin wave energy near the X points in the Brillouin zone, and significantly improving
- agreement with the experimental results. A large energy broadening of the spin wave is needed in
- 133 reproducing the measured spectra, and an additional 10 meV energy broadening is included in the
- simulation. Such damping of the spin wave may come from the frustration in FeGe₂. The simulated (HK0)
- slice at 8 meV (Fig. 1(j)) shows strong "rod" intensity along X-M and only weak intensity along Γ -X near
- the X points for a large range of energy transfer, consistent with the experiments.
- As temperature increases to 300 K, the dispersive magnetic excitations become more and more diffuse and
- soften to lower energy transfer. Constant Q cuts were obtained from the TAX data (Figs. S6(a)-S6(e)),
- revealing a dramatic softening of the spin wave from finite energy at low temperatures to near 0 meV at
- 300 K as seen in Figs. 4 (a), 4(b). This effect is also visible in Fig. 4(c) showing the constant energy scans
- at 8 meV with denser temperature points. Between 5 and 275 K, two peaks between neighboring M points
- can be easily resolved. Above 300 K, the peaks vanish, and the intensity becomes flat between M points.
- 143 Combining these findings, we believe that the well-defined spin wave collapses near 300 K as one enters
- the paramagnetic phase of FeGe₂.
- 145 At the same time as the spin wave collapses, rods of scattering between neighboring M points connect with
- each other and form the checkerboard-shaped diffusive scattering pattern in (HK0) elastic slices of S(**Q**, E).
- To gain a quantitative understanding of the spatial coherence behind these rods, correlation lengths were
- extracted by fitting elastic cuts with a Voigt function across the rod of scattering in the basal plane (Γ-X)
- and across-plane $(\Gamma$ -Z), as described in Supplemental Material. Along the rod direction, the almost flat
- intensity suggests no correlation. At 300 K, the correlation length is about 12 Å in the across-rod direction
- and 23 Å in the across-plane direction, comparable with each other. In this case, 3D order breaks down with
- 2D correlations of plates along directions bisecting the a and b axes remaining in the paramagnetic phase.
- The 2D correlations unveiled in real space are surprising in FeGe₂. In such a quasi-1D system, spins are
- weakly coupled in the a-b plane with fourfold symmetry, and it is expected that correlations in this plane
- disappear simultaneously with only 1D correlation along c axis left. At 500 K, the correlation lengths
- become 4 Å and 11 Å, respectively, indicating a simultaneous decrease of short-range order upon further
- warming into the paramagnetic phase.
- 158 This striking dimension change can also be explained by J₂ and magnetic frustration. Our calculations show
- that a stripe-type configuration has the next-lowest ground state energy, about 3.7 meV per atom above the
- 160 Néel-type AFM structure. When the temperature increases to 300 K, thermal fluctuations become
- 161 comparable to the energy difference between these two configurations and exchange interactions can no
- longer stabilize the Néel-type structure. It is likely that stripe-type domains start to appear and occupy
- nearly half of the system. In the Néel-type structure, the effective coupling along both [1, 1, 0] and [1, -1,
- 164 0] are of $\sim J_1$ -2 J_2 , which is close to zero when $\eta \sim 1$. Once the [1, 1, 0] stripe-type domains are formed, the
- magnitude of effective coupling along [1, -1, 0] remains nearly zero but that along [1, 1, 0] increases to ~
- J_1+2J_2 . In this case the magnetic order could be viewed as plates perpendicular to the rods along [1, -1, 0],
- where there are strong in-plate correlations, but the neighboring plates are nearly decoupled because of the
- where there are strong in-place correlations, but the neighboring places are hearly decoupled occause of the
- small effective correlations between plates. Since [1, 1, 0] and [1, -1, 0] are equivalent directions in the
- system, stripe-type domains along the other direction are equally likely to be formed, together they can
- account for the rods in the checkerboard arrangement.
- 171 In conclusion, we observe anomalous excitations at low temperature, as well as a checkerboard-shaped
- diffusive scattering pattern developing at high temperature. We showed that these two phenomena, though
- different in underling mechanism, both have a magnetic origin and are related to the intraplane NNN
- interaction J₂. This previously ignored interaction generates the extra spin wave feature for a large range of
- the reciprocal space. Our ab initio calculations show J_2 leads directly to the near-perfect in-plane magnetic

- frustration, which facilitates the emergence of unexpected 2D short-range magnetic order at high
- temperature. Low dimensional FeGe₂ has been synthesized for potential spintronic applications [27,28].
- Our revelation of the magnetic frustration and its roles may provide some insights on these studies. Our
- work also sheds light on the potential of controlling the magnetic dimensionality and corresponding
- properties of materials by frustration.

Acknowledgements

181

- Funding: This material is based upon work supported by the National Science Foundation under
- 183 Grant No. 1750786. The neutron scattering portion of this research used resources at the Spallation
- Neutron Source and the High Flux Isotope Reactor, both of which are DOE Office of Science User
- Facilities operated by the Oak Ridge National Laboratory.
- Author Contributions: D.A. and C.L. performed the INS measurements on ARCS. M.S., M.L.
- and C.A. performed the INS measurements on HB-3. Y.S. performed the theoretical calculation.
- Y.S. and C.L. analyzed the data and wrote the manuscript. All authors contributed to discussing
- and editing the manuscript.
- 190 **Competing Interests statement:** The authors declare no competing interests.

191 References

- 192 [1] L. Balents, Spin Liquids in Frustrated Magnets, Nature 464, 199 (2010).
- 193 [2] P. Chandra, P. Coleman, and A. I. Larkin, *Ising Transition in Frustrated Heisenberg Models*, 194 Phys. Rev. Lett. **64**, 88 (1990).
- 195 [3] C. Fang, H. Yao, W. F. Tsai, J. Hu, and S. A. Kivelson, *Theory of Electron Nematic Order in LaFeAsO*, Phys. Rev. B Condens. Matter Mater. Phys. 77, 224509 (2008).
- 197 [4] N. Shannon, T. Momoi, and P. Sindzingre, *Nematic Order in Square Lattice Frustrated Ferromagnets*, Phys. Rev. Lett. **96**, 027213 (2006).
- 199 [5] C. Xu, M. Müller, and S. Sachdev, *Ising and Spin Orders in the Iron-Based Superconductors*, 200 Phys. Rev. B Condens. Matter Mater. Phys. **78**, 020501 (2008).
- 201 [6] B. G. Park, J. Wunderlich, X. Martí, V. Holý, Y. Kurosaki, M. Yamada, H. Yamamoto, A. Nishide, J. Hayakawa, H. Takahashi, A. B. Shick, and T. Jungwirth, *A Spin-Valve-like*
- 203 Magnetoresistance of an Antiferromagnet-Based Tunnel Junction, Nat. Mater. 10, 347 (2011).
- 204 [7] P. Wadley, B. Howells, J. Železný, C. Andrews, V. Hills, R. P. Campion, V. Novák, K. Olejník, F. Maccherozzi, S. S. Dhesi, S. Y. Martin, T. Wagner, J. Wunderlich, F. Freimuth, Y. Mokrousov, J.
- Kuneš, J. S. Chauhan, M. J. Grzybowski, A. W. Rushforth, K. W. Edmonds, B. L. Gallagher, and
- T. Jungwirth, *Electrical Switching of an Antiferromagnet*, Science (80-.). **351**, 587 LP (2016).
- 208 [8] A. T. Wong, C. Beekman, H. Guo, W. Siemons, Z. Gai, E. Arenholz, Y. Takamura, and T. Z.
- Ward, Strain Driven Anisotropic Magnetoresistance in Antiferromagnetic La 0.4Sr0.6MnO3,
- 210 Appl. Phys. Lett. **105**, 052401 (2014).
- 211 [9] Y. Y. Wang, C. Song, B. Cui, G. Y. Wang, F. Zeng, and F. Pan, Room-Temperature
- 212 Perpendicular Exchange Coupling and Tunneling Anisotropic Magnetoresistance in an
- 213 Antiferromagnet-Based Tunnel Junction, Phys. Rev. Lett. 109, 137201 (2012).
- 214 [10] T. Jungwirth, X. Marti, P. Wadley, and J. Wunderlich, *Antiferromagnetic Spintronics*, Nat. Nanotechnol. **11**, 231 (2016).

- 216 [11] K. Yasukōchi, K. Kanematsu, and T. Ohoyama, *Magnetic Properties of Intermetallic Compounds* in *Iron-Germanium System : Fe1.67Ge and FeGe2*, J. Phys. Soc. Japan **16**, 429 (1961).
- 218 [12] E. Krén and P. Szabó, Antiferromagnetic Structure of FeGe2, Phys. Lett. 11, 215 (1964).
- 219 [13] J. B. Forsyth, C. E. Johnson, and P. J. Brown, *The Magnetic Structure and Hyperfine Field of FeGe2*, Philos. Mag. **10**, 713 (1964).
- 221 [14] N. S. Satya Murthy, R. J. Begum, C. S. Somanathan, and M. R. L. N. Murthy, *Magnetic Structures in the Iron-Germanium System*, Solid State Commun. **3**, 113 (1965).
- 223 [15] E. F. Bertaut and J. Chenavas, *Comments on the Magnetic Structure of ∂-FeGe2*, Solid State Commun. **3**, 117 (1965).
- 225 [16] J. Sólyom and E. Krén, On the Magnetic Structure of FeGe2, Solid State Commun. 4, 255 (1966).
- V. V Tarasenko, V. Pluzhnikov, and E. Fawcett, *Theory of the Magnetic Phase Diagram and Magnetostriction of FeGe2*, Phys. Rev. B 40, 471 (1989).
- [18] T. M. Holden, A. Z. Menshikov, and E. Fawcett, *Anisotropic Spin-Wave Dispersion in FeGe2*, J.
 Phys. Condens. Matter 8, L291 (1996).
- [19] C. P. Adams, T. E. Mason, E. Fawcett, A. Z. Menshikov, C. D. Frost, J. B. Forsyth, T. G. Perring, and T. M. Holden, *High-Energy Magnetic Excitations and Anomalous Spin-Wave Damping in FeGe2*, J. Phys. Condens. Matter 12, 8487 (2000).
- 233 [20] H. Zhou, Room Temperature Section of the Phase Diagram of the Cu-Fe-Ge Ternary System, J. Less-Common Met. 171, 113 (1991).
- 235 [21] L. M. Corliss, J. M. Hastings, W. Kunnmann, R. Thomas, J. Zhuang, R. Butera, and D. Mukamel, 236 *Magnetic Structure and Critical Properties of FeGe2*, Phys. Rev. B **31**, 4337 (1985).
- 237 [22] H. L. Smith, Y. Shen, D. S. Kim, F. C. Yang, C. P. Adams, C. W. Li, D. L. Abernathy, M. B. Stone, and B. Fultz, *Temperature Dependence of Phonons in FeGe2*, Phys. Rev. Mater. **2**, 103602 (2018).
- [23] G. Henkelman, A. Arnaldsson, and H. Jónsson, A Fast and Robust Algorithm for Bader
 Decomposition of Charge Density, Comput. Mater. Sci. 36, 354 (2006).
- 242 [24] N. Shannon, B. Schmidt, K. Penc, and P. Thalmeier, *Finite Temperature Properties and Frustrated Ferromagnetism in a Square Lattice Heisenberg Model*, Eur. Phys. J. B **38**, 599 (2004).
- 244 [25] D. C. Johnston, *The Puzzle of High Temperature Superconductivity in Layered Iron Pnictides and Chalcogenides*, Advances in Physics.
- [26] A. Sapkota, B. G. Ueland, V. K. Anand, N. S. Sangeetha, D. L. Abernathy, M. B. Stone, J. L.
 Niedziela, D. C. Johnston, A. Kreyssig, A. I. Goldman, and R. J. McQueeney, *Effective One-Dimensional Coupling in the Highly Frustrated Square-Lattice Itinerant Magnet CaCo2-YAs2*,
 Phys. Rev. Lett. 119, (2017).
- [27] D. Czubak, S. Gaucher, L. Oppermann, J. Herfort, K. Zollner, J. Fabian, H. T. Grahn, and M.
 Ramsteiner, Electronic and Magnetic Properties of α-FeGe2 Films Embedded in Vertical Spin
 Valve Devices, Phys. Rev. Mater. 4, 104415 (2020).
- 253 [28] S. Tang, I. Kravchenko, T. Z. Ward, Q. Zou, J. Yi, C. Ma, M. Chi, G. Cao, A.-P. Li, D. Mandrus, and Z. Gai, *Dimensionality Effects in FeGe2 Nanowires: Enhanced Anisotropic Magnetization and Anomalous Electrical Transport*, Sci. Rep. 7, 7126 (2017).

Figures and Tables

258

FIG. 1. Checkerboard-shaped anomaly is observed in the (HK0) planes.

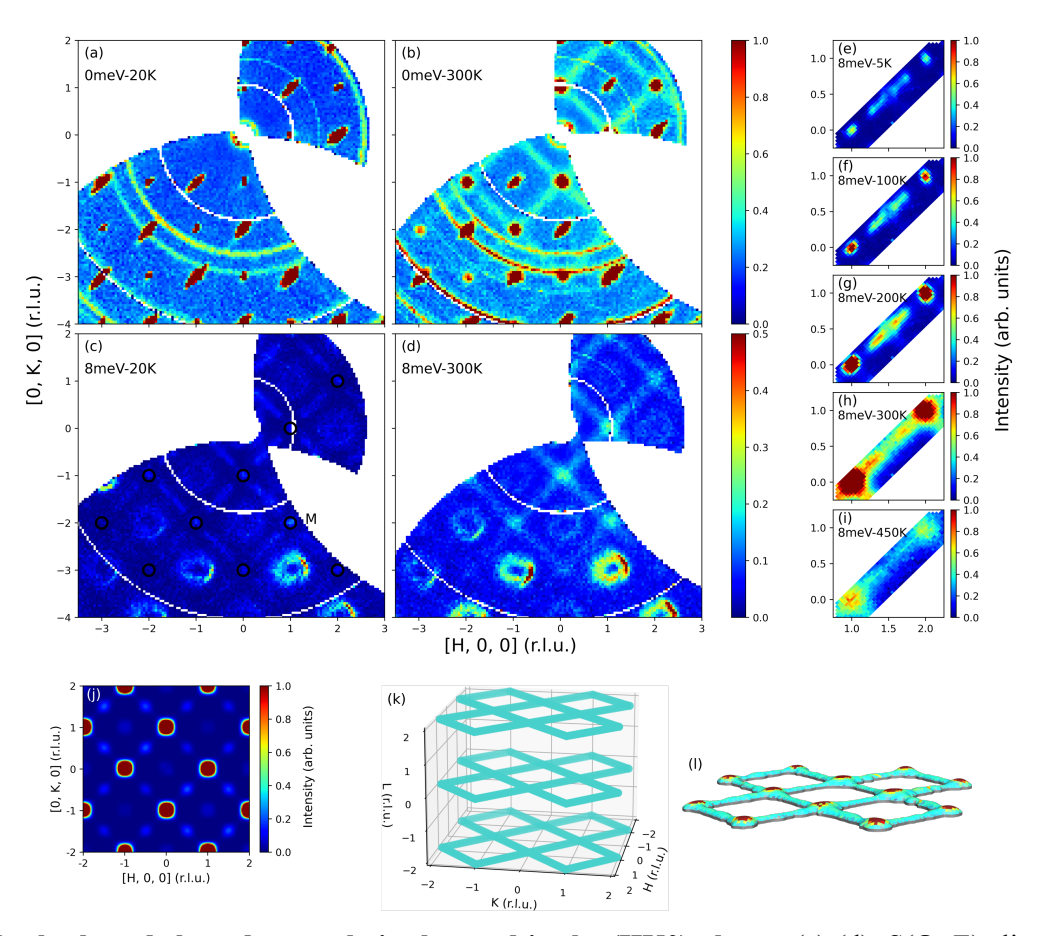


FIG. 1. Checkerboard-shaped anomaly is observed in the (HK0) planes. (a)-(d): $S(\mathbf{Q}, E)$ slices from ARCS measurements, obtained by integrating [-0.5, 0.5] meV in energy and [-0.1, 0.1] reciprocal lattice units (r.l.u.) along [0, 0, L]. (a)(b): Elastic scattering results, (c)(d): inelastic scattering results with a neutron energy loss of 8 meV. In (a)(b), those peaks with H+K even are nuclear Bragg peaks (Γ), and those with H+K odd are magnetic Bragg peaks (M). In general, the intensities of nuclear Bragg peaks are stronger than that of magnetic ones and will increase with respect to the absolute value of momentum transfer |**Q**|. The intensities of magnetic Bragg peaks are, on the other hand, weaker at larger |**Q**|. (e)-(i): $S(\mathbf{Q}, E)$ slices from TAX measurements, which is more limited but has better resolution. (j): Spin wave simulation of (HK0) plane at 8 meV from NNN model. (k): Three-dimensional (3D) schematic of the checkerboard-shaped anomaly. (l): 3D rendering of L=0 schematic.



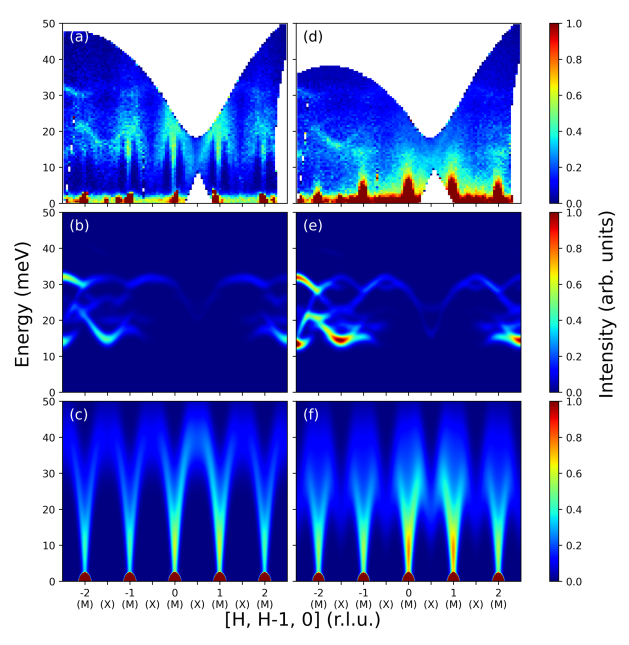


FIG. 2. Dispersive scattering intensity in several Brillouin zones in slices along [H, H-1, 0]. (a)(b) 20K. (d)(e) 300K. (a) and (d) are S(Q, E) slices from ARCS measurements, obtained by integrating [-0.1, 0.1] r.l.u. along [0, 0, L] and [-0.05, 0.05] r.l.u. along [H, -H, 0]. (b)(e) are simulated phonons. (c)(f) are simulated spin waves from the NN model and NNN model.

FIG. 3. The $|\mathbf{Q}|$ -dependence of the checkerboard-shaped anomaly matches well with magnetic form factor of Fe.

260

261

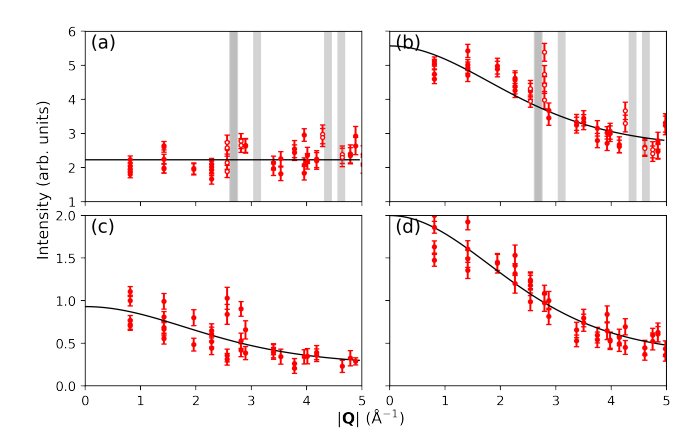


FIG. 3. The |Q|-dependence of the checkerboard-shaped anomaly matches well with magnetic form factor of Fe. The fittings were done on 20 K (a)(c) and 300 K (b)(d) ARCS data for energy transfer of 0 meV (a)(b) and 8 meV (c)(d). The red solid circles are experimental data used for fitting, and the black solid lines are the fitted results. The gray vertical stripes in (a)(b) are places where data points were excluded (red open circles) due to the sample environment background.

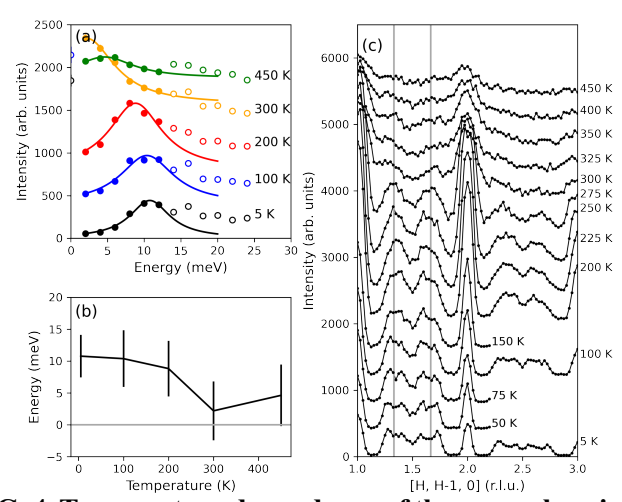


FIG. 4. Temperature dependence of the anomalous intensity along [H, H-1, 0]. (a) Constant Q cuts at [1.6, 0.6, 0] from TAX data. (b) Lorentzian fit to the first peak (solid circles) in (a), error bars represent the full width at half maximum. (c) Constant E scans along [H, H-1, 0] at 8 meV with the black solid lines as guides to the eye. The vertical gray lines indicate peaks at about 1 and 2 r.l.u.. Error bars are smaller than the symbols.

Table I. Parameters obtained from total energy calculations.

Model	J_1S^2	J_2S^2	J_cS^2	η
	(meV)	(meV)	(meV)	
NN	-7.2 ± 2.2	-	83 ± 4	-
NNN	-7.2 ± 0.5	-2.6 ± 0.4	81.1 ± 0.9	1.4